# Magnetic and elastic properties of $CoFe_2O_4$- polydimethylsiloxane magnetically oriented elastomer nanocomposites

P. Soledad Antonel, Guillermo Jorge, Oscar E. Perez, Alejandro Butera, A. Gabriela Leyva, and R. Martín Negri

Citation: Journal of Applied Physics **110**, 043920 (2011); doi: 10.1063/1.3624602
View online: https://doi.org/10.1063/1.3624602
View Table of Contents: http://aip.scitation.org/toc/jap/110/4
Published by the American Institute of Physics

# Magnetic and elastic properties of $CoFe_2O_4$- polydimethylsiloxane magnetically oriented elastomer nanocomposites

P. Soledad Antonel,[1] Guillermo Jorge,[2] Oscar E. Perez,[3] Alejandro Butera,[4] A. Gabriela Leyva,[5] and R. Martín Negri[1,a)]

[1]*Instituto de Química Física de Materiales, Ambiente y Energía (INQUIMAE). Departamento de Química Inorgánica, Analítica y Química Física. Facultad de Ciencias Exactas y Naturales, Universidad de Buenos Aires, Buenos Aires C1428EGA, Argentina*

[2]*Departamento de Física. Facultad de Ciencias Exactas y Naturales, Universidad de Buenos Aires, Buenos Aires, C1428EGA, Argentina*

[3]*Departamento de Industrias. Facultad de Ciencias Exactas y Naturales. Universidad de Buenos Aires, Buenos Aires C1428EGA, Argentina*

[4]*Centro Atómico Bariloche (Comisión Nacional de Energía Atómica. Argentina) and Instituto Balseiro, Universidad Nacional de Cuyo, Bariloche, Río Negro, Argentina*

[5]*Departamento de Física de la Materia Condensada. Gerencia de Investigación y Aplicaciones. Centro Atómico Constituyentes, Comisión Nacional de Energía Atómica and Escuela de Ciencia y Tecnología, UNSAM, Argentina*

(Received 14 December 2010; accepted 4 July 2011; published online 25 August 2011)

Magnetic elastic structured composites were prepared by using $CoFe_2O_4$ ferromagnetic and superparamagnetic nanoparticles as fillers in polydimethylsiloxane (PDMS) matrixes, which were cured in the presence of a uniform magnetic field. Cobalt-iron oxide nanoparticles of three different average sizes (between 2 and 12 nm) were synthesized and characterized. The smallest nanoparticles presented superparamagnetic behavior, with a blocking temperature of approximately 75 K, while larger particles are already blocked at room temperature. Macroscopically structured-anisotropic PDMS-$CoFe_2O_4$ composites were obtained when curing the dispersion of the nanoparticles in the presence of a uniform magnetic field (0.3 T). The formation of the particle's chains (needles) orientated in the direction of the magnetic field was observed only when loading with the larger magnetically blocked nanoparticles. The SEM images show that the needles are formed by groups of nanoparticles which retain their original average size. The Young's moduli of the structured composites are four times larger when measured along the oriented needles than in the perpendicular direction. Magnetization (VSM) and ferromagnetic resonance curves of the structured composites were determined as a function of the relative orientation between the needles and the probe field. The remanence magnetization was 30% higher when measured parallel to the needles, while the coercive field remains isotropic. These observations are discussed in terms of the individual nanoparticle's properties and its aggregation in the composites. © *2011 American Institute of Physics*. [doi:10.1063/1.3624602]

## I. INTRODUCTION

Magnetorheological compounds are produced by dispersions of magnetic particles into viscoelastic systems, including elastomeric polymers.[1–11] The possibility of inducing anisotropic properties by the action of magnetic fields[5–7,12–14] is of great interest for its potential application in sensors and actuators.[10] However, the applications of magnetorheological materials are at an early stage.[15,16] Most of the articles are concerned with magneto fluids, such as silicon oils or other high viscosity fluids, however, there are few studies using cured polymers with the application of magnetic fields during curing.[5–7,15] Pioneering characterization works using magnetite and carbonyl iron particles, with micrometric sizes, have been reviewed by Filipcsei *et al.*[5] Nevertheless, the use of other compounds with different sizes (particularly nanoparticles) and magnetic properties (in the superparamagnetic state) has not yet been studied. Topics such as the influence of the magnetic state and the properties of the particles on the morphological structure of the final oriented composite are far from being clarified.

Nanoparticles of cobalt-iron oxides are very interesting compounds for magnetorheological materials, because they present a relatively large magnetic anisotropy, moderate-high magnetization, and high coercivity at room temperature.[17] The possibility of modulating the magnetic properties by synthesizing nanoparticles of different sizes also appears to be interesting feature. However, cobalt ferrites have not yet been explored in magnetoelasticity and the use of nanoparticles rather than microparticles has not yet received attention. Therefore, both the elastic and magnetic properties of magnetically structured $CoFe_2O_4$ nanoparticles-PDMS cured composites are presented and discussed in this work.

## II. EXPERIMENTAL SECTION

### A. Synthesis of $CoFe_2O_4$ nanoparticles

Among the reported methods for the preparation of $CoFe_2O_4$ nanocrystals,[18–22] chemical co-precipitation is the

a)Author to whom correspondence should be addressed. Electronic mail: rmn@qi.fcen.uba.ar.

 

most widely used,[20–23] and it was used here. Following Kim *et al.*,[20] 22.25 mL of a solution mixture of $FeCl_3.6\ H_2O$ 0.450 M and $CoCl_2.6\ H_2O$ 0.225 M (2:1), in 0.4 M HCl, was added drop-by-drop to 200 mL of 1.5 M NaOH, previously adjusted to $p\mathrm{H} = 12$, at high speed stirring. The synthesis temperature was controlled by a water-jacketed reaction vessel using circulating thermostatic bath. The precipitation of dark brown $CoFe_2O_4$ nanoparticles occurred immediately and both high speed stirring and the desired temperature were maintained during the addition of the cationic mixture. The obtained precipitates were kept vigorously stirred at the desired temperature for 2 h. The synthetic procedure described in the preceding text was performed at open atmosphere.

Then $CoFe_2O_4$ nanoparticles were separated from the reaction medium by centrifugation at approximately 12 000 G for 20 min. The resulting precipitates were washed with MilliQ water, and the washing and centrifugation cycles (always at 12 000 G) were repeated until the *p*H of the supernatant was nearly 7 (approximately 10 cycles of washing and centrifugation). It was confirmed by XRD that 10 cycles of washing and centrifugation also eliminates NaCl, which was present in the reaction medium due to the solutions used in the synthesis. If fewer cycles of washing/centrifugation were performed, the characteristics peaks of NaCl are also present in the diffractograms.

Finally, $CoFe_2O_4$ nanoparticles were dried using a vacuum oven, at 40 °C for 24 h. This synthesis was repeated at three different temperatures (40, 60, and 80 °C), in order to obtain nanoparticles of different sizes and magnetic properties.

### B. Preparation of PDMS-$CoFe_2O_4$ composites

The PDMS base and crosslinker agent (Sylgar 184, Dow Corning) were mixed in proportions of 1:10 (*w*/*w*) at room temperature and then loaded with the magnetic nanoparticles, in different proportions. Specifically, composites with 5 and 10% *w*/*w* of the $CoFe_2O_4$ nanoparticles synthesized at 80 °C were prepared, while for the nanoparticles synthesized at 40 °C, only 5% composites were prepared.

This mixture, still fluid, was placed for curing inside a cylindrical mold (dimensions: $1 \times 3$ cm). The mold is part of a designed device which allows the curing of the samples at a given temperature in the presence of an applied magnetic field, while rotating the sample at a constant speed (approximately 30 rpm) for homogenizing (see Supplementary Material[35]). The samples were cured inside the mold at $75 \pm 5$ °C in the presence of a uniform magnetic field (0.3 T) during 4 h. A uniform magnetic field of 0.3 T was generated in a $1 \times 3$ cm volume with a standard Varian low impedance electromagnet (model V3703) provided with a set of pole pieces with a diameter of 10 cm. These kinds of electromagnets are known to provide highly homogeneous steady magnetic fields.

In addition, a composite with 5% *w*/*w* of magnetic nanoparticles was cured without an applied magnetic field for comparison.

### C. XRD, TEM and SEM

X-ray powder diffraction analysis (XRD) of the nanoparticles was performed with a Philips X-Pert diffractometer using Cu $K_\alpha$ radiation ($\lambda = 0.154056$ nm) and the average size of the crystallites were determined by the Scherrer equation. A transmission electron microscope, (TEM) (Philips EM 301) was employed to examine the morphology and also the size of the nanoparticles. The size distribution was determined in each case by counting 200 particles. The morphology of the PDMS-$CoFe_2O_4$ composites was studied using a field emission scanning electron microscope (Zeiss Supra 40 Gemini). Energy-dispersive x-ray spectroscopy (EDS) experiments were performed with the same equipment.

### D. Magnetic properties of nanoparticles and composites

A LakeShore 7400 vibrating sample magnetometer (VSM) was used for recording the magnetization curves at room temperature. Zero field cooling (ZFC) and field cooling curves were recorded in a superconducting quantum interference device (SQUID) magnetometer (Quantum Design MPMS XL). Ferromagnetic-resonance (FMR) spectra of the composites were taken in a Bruker ESP-300 spectrometer at room temperature.

### E. Texture analysis

Samples for texture analysis were prepared by cutting the cured composites in the directions transversal and longitudinal to the main axis of the mold's cylinder (coincident with the direction of the applied magnetic field during curing). A specially designed holder was used for cutting the cured composites in order to obtain pieces of equal thickness (2 mm) and similar areas (0.78 and 0.83 $cm^2$) in both directions, parallel and perpendicular to the applied magnetic field during curing (that is, in the direction of the needles). The piece can rigidly hold the cured composite and allows for the introduction of a surgical scalpel through specially designed slots with a thickness equal to the thickness of the scalpel. The slots are placed in different positions through the holder. In this way, it is possible to make cuts in different directions matching the thickness and areas of the cut pieces without deforming and assuring parallel faces.

The texture analysis was performed using a Stable Microsystems TA-XT2i texture analyzer which compresses the sample at a constant compression speed (100 $\mu$m/s) in the range between 8 to 30% of the initial thickness.[24] Different compression-decompression cycles were performed at least in duplicate to characterize the material recovery, possible rupture, or hysteresis. These experiments allows recovery of the Young's modulus, *E,* in the different orientations.

## III. RESULTS AND DISCUSSION

### A. Characterization of $CoFe_2O_4$ nanoparticles

Figure 1 shows a TEM image of $CoFe_2O_4$ nanoparticles prepared at 80 °C (co-precipitation temperature). The TEM images of the nanoparticles synthesized at 40 and 60 °C are very similar, so they are not shown here. In all cases, the size distributions obtained by TEM have maxima between 1-2, 9-10, and 11-12 nm for synthesis performed at 40, 60, and 80 °C, respectively (see histograms in the Supplementary

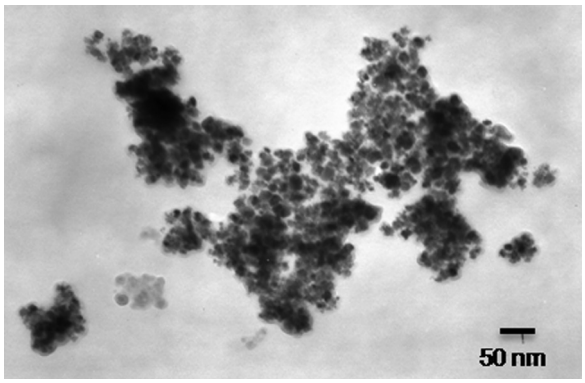


FIG. 1. TEM images of $CoFe_2O_4$ nanoparticles prepared at T = 80 °C.

Material[35]). The increase in the mean particle size with the temperature of synthesis is in good agreement with recently reported works.[20,25,26] The particles appear as nearly spherical in the recorded TEM images.

X-ray powder diffraction patterns (XRD, Fig. 2) indicate that the synthesized $CoFe_2O_4$ nanoparticles at 60 and 80 °C are crystalline single phases. The x-ray diffraction peaks correspond to the cubic inverse spinel type lattice, as expected for $CoFe_2O_4$ (ICDD 03-0864). Additionally, energy-dispersive x-ray spectroscopy (EDS) experiments were performed for all samples, always finding excellent agreement in the Co/Fe molar ratio obtained, comparing with those expected from the $CoFe_2O_4$ stoichiometry.

The nanoparticles synthesized at 40 °C show broad and unresolved peaks. The degree of crystalline character increases with the temperature of synthesis. In the case of the nanoparticles obtained at 60 and 80 °C, the mean crystallite sizes were estimated from the more intense peaks, (220), (311), and (400), using the Scherrer equation. The calculated average size of the crystallites are 10-11 nm and 17-22 nm for the nanoparticles synthesized at 60 and 80 °C, respectively, in agreement with the TEM results. No crystalline size was calculated for the samples synthesized at 40 °C since the diffractogram shows low crystallinity.

The magnetic characterization of the nanoparticles at room temperature is presented in Fig. 3(a), where the M versus H curves (VSM) for three different temperatures of synthesis are shown. As the size of the particles increases it is

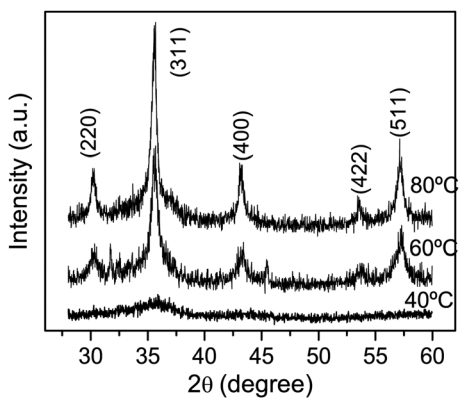


FIG. 2. XRD patterns of the $CoFe_2O_4$ nanoparticles synthesized at 40, 60, and 80 °C.

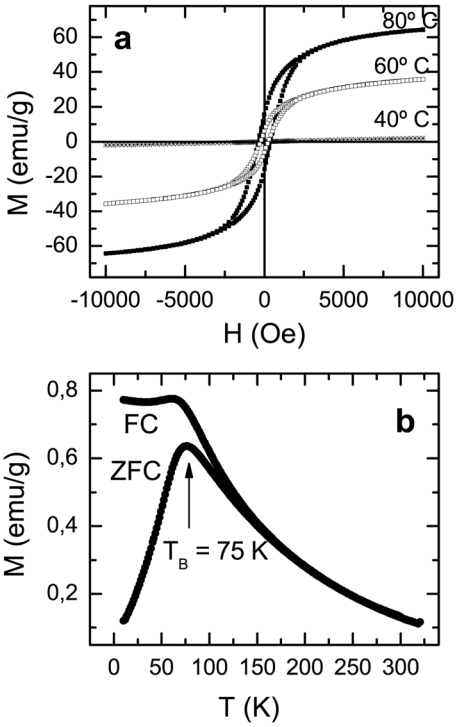


FIG. 3. (a) Magnetic hysteresis curves at 25 °C for the $CoFe_2O_4$ nanoparticles synthesized at 40, 60, and 80 °C. (b) ZFC and FC magnetization vs temperature curves (H = 0.05 T) for the $CoFe_2O_4$ nanoparticles synthesized at 40 °C.

clear that the saturation magnetization ($M_s$), remanence magnetization ($M_r$), and coercive field ($H_c$) systematically increase with the temperature of synthesis. This increment was previously assigned to a greater degree of crystallinity.[27] It is also clear from the figure that the smaller particles (obtained at 40 °C) have a superparamagnetic behavior, whereas larger particles are blocked at room temperature. It is known that $CoFe_2O_4$ particles smaller than 35 nm are in a magnetic monodomain regime,[23] thus all of the synthesized particles are expected to be magnetic monodomains. This is confirmed by the fact that increasing the particle size yields to enhanced coercive fields (an indication of monodomain regime according to Leslie-Pelecky *et al.*[28]) and the saturation magnetization tends to approach the bulk value of 73 emu/g.[23]

The (SQUID) M versus T curves for the particles synthesized at 40 °C (2 nm size) are presented in Fig. 3(b). The ZFC (zero field cooling) and FC (field cooling) curves show the typical change of regime from the superparamagnetic to the blocked state. A maximum in the ZFC curve is observed, which is identified with the blocking temperature, $T_B$, of these particles ($T_B$ = 75 K, similar to the value reported by Kim and co-workers).[20] It is concluded that the smallest nanoparticles (2 nm) are in the superparamagnetic state at room temperature with a blocking temperature of about 75 K.

### B. Morphology and magnetic properties of anisotropic PDMS-$CoFe_2O_4$ composites

The device designed for curing the composites in the presence of a uniform magnetic field is described in the

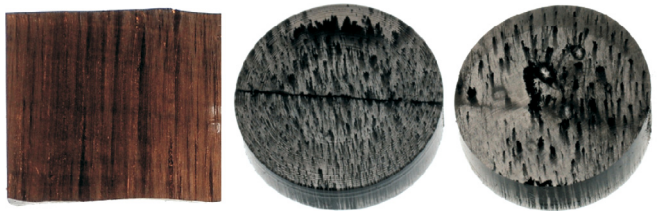

FIG. 4. (Color online) Photographs of the magnetically aligned needles of $CoFe_2O_4$ nanoparticles in PDMS composites (5 and 10% *w*/*w* of filler nanoparticles) which were cured in the presence of a magnetic field.

Supplementary Material.[35] The formation of macroscopic needles of inorganic material, observed by the naked eye and oriented along the direction of the magnetic field, was obtained when curing in the presence of the field (Fig. 4), for both 5% and 10% *w*/*w* of $CoFe_2O_4$ nanoparticles synthesized at 80° C. In the absence of the external magnetic field, composites with a uniform distribution of nanoparticles, without the presence of macroscopic needles, were obtained. The formation of needles was detected only in the case of curing with an applied field (see SEM images in the Supplementary Material,[35] showing composites cured in presence and absence of a magnetic field, for comparison). Moreover, it is remarked that the needles are always oriented in the direction of the field. The SEM images of the needles are shown in Fig. 5.

On the contrary, composites prepared with the nanoparticles obtained at 40 °C in the presence of an external magnetic field (0.3 T) do not show the formation of needles. Therefore, in this case the nanoparticles are randomly distributed. This shows that the magnetic interaction between such nanoparticles is not strong enough to promote the formation of needles at the present experimental conditions. These findings confirm that the formation of needles is due to the presence of magnetic nanoparticles having the appropriate magnetic properties to interact with the external magnetic field during curing. A composite with a random distribution of nanoparticles (no needle formation) is obtained when no magnetic field is applied during curing or when the particles with the lower magnetic moment are used (those synthesized at 40 °C).

In the case of the ferromagnetic (magnetically blocked) nanoparticles synthesized at 80 °C, the SEM images shown in Fig. 5 illustrate several features of the composites prepared in the presence of the magnetic field. First, almost all of the nanoparticles are in the needles since no particles were detected in other regions of the material. Second, the chains (needles) are formed by individual particles, (almost monodisperse) whose sizes are very similar to those of the synthesized $CoFe_2O_4$ nanoparticles (observed in TEM images). This means that the nanoparticles keep their identity as individual particles and are grouped, forming needles, when curing the composite in the presence of the magnetic field. In Figs. 5(a) and 5(b) examples of top views of the needles, for 10 and 5% *w*/*w* in the magnetic nanoparticles,

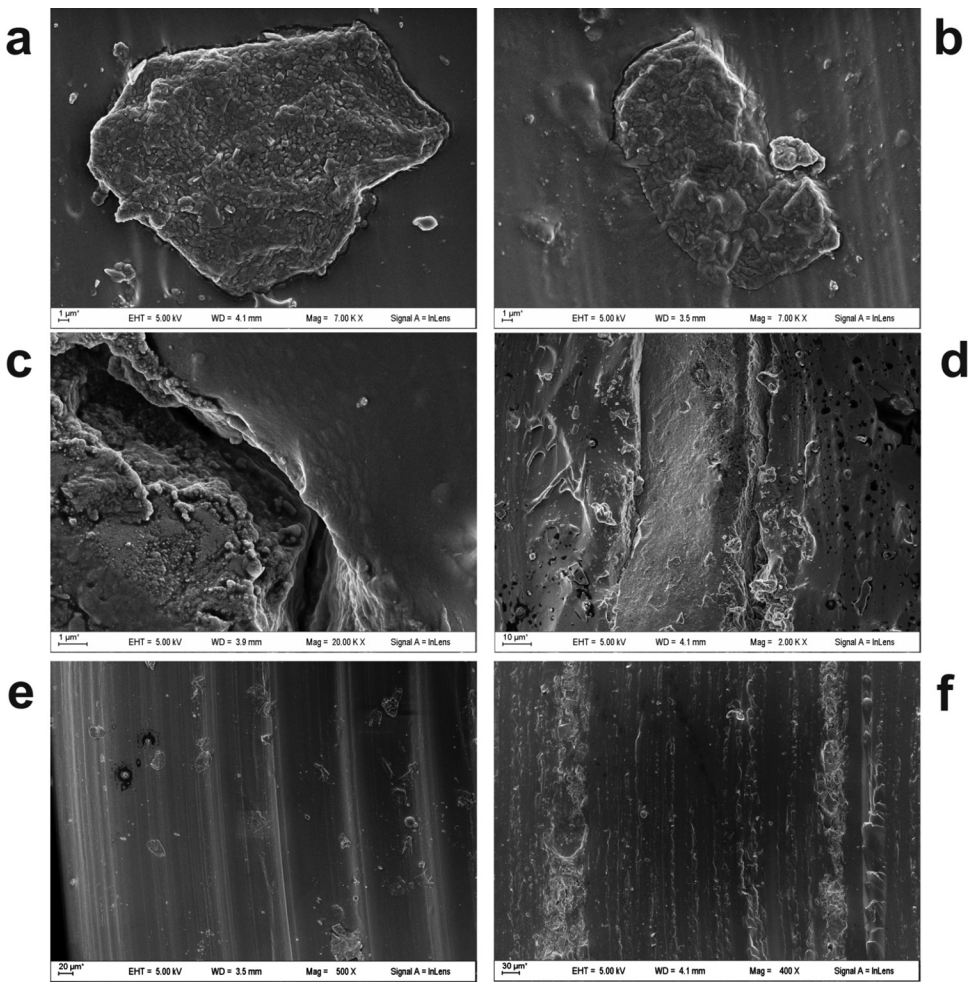


FIG. 5. SEM images of the structured PDMS-$CoFe_2O_4$ composites. (a) Inorganic needle (top view), 10% *w*/*w* of $CoFe_2O_4$, dimensions: $23.6 \times 33.9$ $\mu$m. (b) Inorganic needle (top view), 5% *w*/*w* of $CoFe_2O_4$, dimensions: $12.4 \times 24.1$ $\mu$m. (c) Interface between needle and PDMS. (d) Inorganic needle (lateral view). (e) Panoramic top view of needles in the composite. (f) Panoramic lateral view of needles in the composite.

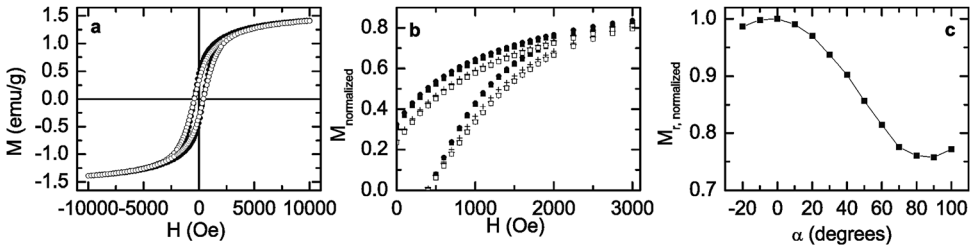


FIG. 6. Magnetization curves of structured composites, as a function of the relative angle ($\alpha$) between the needle alignment and the VSM-sensing field. (a) Filler concentration 5% *w/w*: —●—, $\alpha = 0°$; —○—, $\alpha = 90°$. (b) Detail in the $M_r$ zone of the normalized magnetization ($M/M_{sat}$) for $\alpha = 0$ and 90°; ■,10% *w/w* $\alpha = 0°$; □, 10% *w/w* $\alpha = 90°$; ●, 5% *w/w* $\alpha = 0°$; ○, 5% *w/w* $\alpha = 90°$; +, powder of nanoparticles. (c) Relative (to $\alpha = 0$) remanent magnetization vs $\alpha$ (10% *w/w*).

respectively, are presented. The dimensions of the needles depend upon the concentration of $CoFe_2O_4$ in the composite. In the case of 10% *w/w* (Fig. 5(a)), the average dimensions are $23.6 \times 33.9$ $\mu$m, while for the 5% *w/w* they are $12.4 \times 24.1$ $\mu$m, respectively (Fig. 5(b)). Therefore, the width of the needles increases with the concentration of the $CoFe_2O_4$ nanoparticles, at a constant applied magnetic field during curing.

Figure 5(c) illustrates the boundary between a needle and the PDMS. A lateral view of the needle is presented in Fig. 5(d). Figures 5(e) and 5(f) show panoramic SEM images of the composites, with several needles dispersed in the PDMS matrix.

Having obtained a macroscopically anisotropic material, the magnetic behavior for different orientations was measured. The magnetization curves of the structured composites were measured as a function of the relative angle, $\alpha$, between the needle's alignment and the VSM-sensing field. In particular, Figs. 6(a) and 6(b) show magnetic hysteresis cycles for $\alpha = 0$ and 90°, which correspond to the parallel and perpendicular orientations between the needles and the sensing field. Both curves have identical shapes and are also similar to those of the powder. This indicates that the nanoparticles keep their individual characteristics, which is in agreement with the results of TEM and SEM.

Superimposed on these similarities, we also observed some minor but systematic differences of the magnetization curves as a function of $\alpha$. In order to visualize these differences, detailed normalized magnetization ($M_{normalized}$) curves are presented in Fig. 6(b) for $\alpha = 0°$ and 90°. No demagnetizing factor was used for correcting the VSM data measured as a function of $\alpha$. In order to check for possible geometric artifacts, VSM magnetization measurements were performed with two 5% *w/w* composites, both with the same parallelepiped shape ($1 \times 3 \times 10$ mm$^3$); one of them cured with an applied field of 0.3 T, and the other cured in the absence of the applied field. In both samples hysteresis loops were measured, with applied fields perpendicular and parallel to the needles (for the latter) and to the main face (for the former, in which no needles are formed). For the sample cured in the presence of an applied magnetic field, a difference in the remanence ratio ($M_r/M_s$) between the two curves was obtained. Nevertheless, no difference in the remanence ratio is observed in the zero-field cured composite, which is an indication that demagnetizing fields are not involved in the effect shown in Fig. 6(c).

Additionally, it is observed in Fig. 6 that $M_{normalized}$ is larger for $\alpha = 0$ in the whole range of the sensing field, both for the 5 and 10% composites. This effect is clearly observed when a scan of the normalized remanence magnetization (relative to its value at $\alpha = 0$), $M_{r,normalized}$, as a function of $\alpha$, is performed (Fig. 6(c)), noting a difference of about 25% in the remanence magnetization between $\alpha = 0$ and 90°. Moreover, a cosine-square-like behavior is observed, with a maximum for $\alpha = 0°$ and a minimum for $\alpha = 90°$.

The characteristics observed in Figs. 6(b) and 6(c) indicate a certain degree of magnetic structuring of the composite. These results are in agreement with ferromagnetic-resonance (FMR) spectra (Fig. 7) for 10% *w/w* composites, which were measured at 24.1 GHz in the directions parallel and

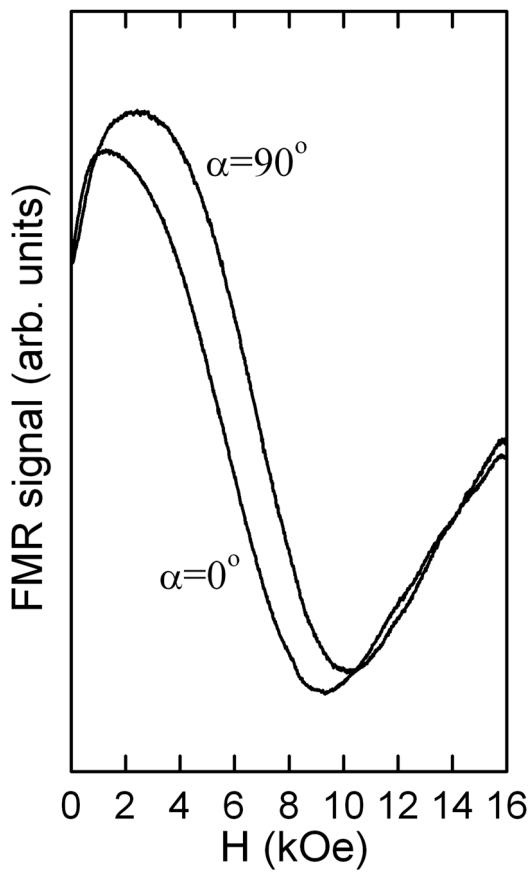


FIG. 7. FMR curves measured at 24.13 GHz with the external field applied parallel ($\alpha = 0°$) or perpendicular ($\alpha = 90°$) to the needles. If no field is applied during the curing of the samples, both spectra are coincident.

perpendicular to the needles ($\alpha = 0°$ and 90°, respectively). Measurements at lower frequencies (9.5 GHz) showed similar results, but were more difficult to model due to the very large linewidth. The difference between the resonance fields in both orientations indicates that there is some degree of magnetic anisotropy that could be related to the agglomeration of the nanoparticles in the shape of a needle. This difference in the resonance field of approximately 900 Oe was not observed in the control composites fabricated in zero field. In the case of uniaxial anisotropy, it is possible to relate[29] the resonance field in the parallel and perpendicular directions with the shape magnetic anisotropy, $H_r(90°) - H_r(0°) = (3/2)\ 2\pi M_s \sim 3800$ Oe (we have used the reported value for Co-ferrites, $M_s = 400$ emu/cm$^3$; see Ref. 30). It is then deduced that the measured anisotropy is considerable lower than the expected value for perfect needles, indicating that the interactions among the agglomerated nanoparticles are not strong enough to induce a collective needle-like magnetic behavior. Moreover, note that if the particles are not perfect spheres this anisotropy could be due to a partial alignment of the large axis of the individual particles with the external field.

In the previous discussion we have assumed that the magnetocrystalline anisotropy of each particle is randomly distributed. If this is the case, the relatively large crystalline anisotropy in $CoFe_2O_4$ ($K = 1-4 \times 10^6$ erg/cm$^3$; see Ref. 30), should produce a considerably larger linewidth. In the case of a random distribution of particles with cubic anisotropy, the linewidth can be estimated to be $\Delta H_{pp} \sim 2 \times 2\ K/M_s$; see Ref. 31 (this approximation is valid in the limit of relatively low anisotropy; for the general case, see Ref. 31). We have measured a linewidth of $\Delta H_{pp} \sim 9000$ Oe in the sample of Fig. 7, which is even larger in the case of randomly distributed particles ($\Delta H_{pp} \sim 11000$ Oe in this case). Using the reported values, $K = 1 \times 10^6$ erg/cm$^3$ and $M_s = 400$ emu/cm$^3$, the expected linewidth should be in the range of $\Delta H_{pp} \sim 10\ 000$ Oe, which is totally consistent with the results we have found, indicating that the axes of the crystallites are almost randomly oriented, even in the case of the samples fabricated under an applied field.

In summary, these results show that from the magnetic point of view the structured composites have a small, but not null magnetic anisotropy, as was reported recently for another system,[32] which probably originated in the partial alignment of individual nanoparticles with the external field, and is not due to a magnetic needle-like collective behavior.

### C. Young's modulus and elastic behavior of PDMS-$CoFe_2O_4$ composites

The last issue we discuss is regarding the changes in the elastic properties of the elastomeric composites due to the presence of the oriented needles. We use the so-called texture analyzer for exploring the elastic features and finally determining the Young's modulus of the composites in both directions, parallel and perpendicular to the needles, referred to as $E_{\|}$ and $E_{\perp}$, respectively. Analogously, in the following discussion the thickness of the samples, when compressed in the directions parallel or perpendicular to the needles, are referred as $L_{\|}$ and $L_{\perp}$, respectively, while the symbol, L, stands, generically, for the thickness of the sample without considering in which direction the stress was exerted.

Figure 8(a) shows the typical behavior of a composite under repeated compression, in force versus time curves, in which three cycles of slow-compression and fast-decompression are illustrated. The curves are presented as directly obtained from the texture analyzer in cycles of slow compression at a constant speed ($v = 100$ $\mu$m/s) reaching up to 30% of the initial thickness ($L_i$), followed by fast decompression (instantaneous in the time scale of the experiment). During that compression, the equipment records the force (F) required to keep the speed of compression constant ($v$) as a function of time (t). These curves can be fitted if we assume that the sample follows Young's law which relates the strain with the pressure ($P = F/A$; $A$ = area perpendicular to the direction of compression) in the direction of compression, dL/

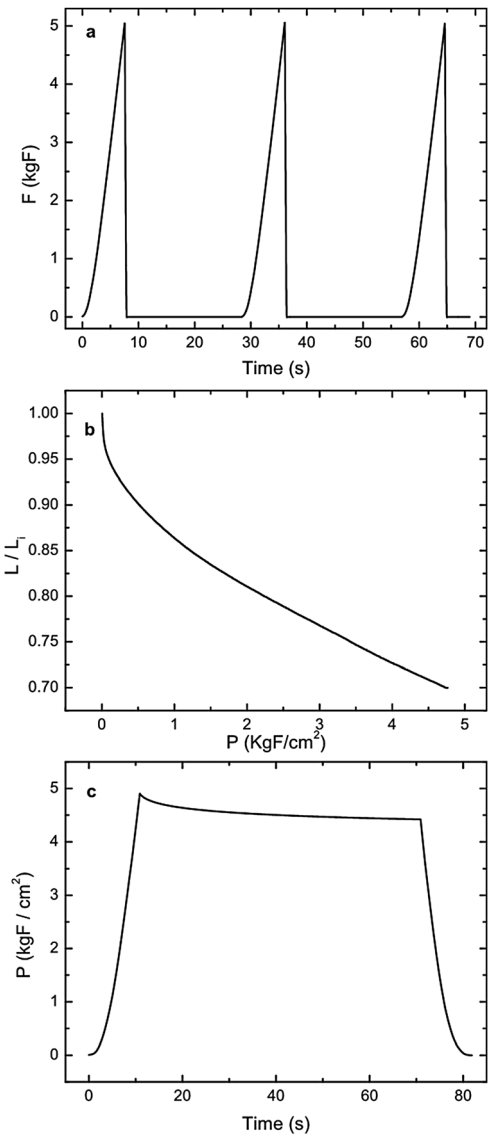


FIG. 8. Elasticity results for a 10% *w/w* composite measured in the direction parallel to the needles. (a) Cycles of force (F) vs compression time (t) (speed of compression $v = 100$ $\mu$m/s; maximum strain: 30%). (b): $L_{\|}/L_i$ vs P. (c) Relaxation curve: the sample is compressed up to a 30% strain under the same conditions as in (a), and then the compression probe is kept at that strain for 60 s.

$L = -dP/E$, where L is the thickness of the sample ($L = L_i - vt$) and E is Young's modulus (the variable time (t) is related to the strain $\epsilon$ ($\varepsilon \equiv \Delta L/L_i$) by $\varepsilon = (vt/L_i)$. Hence, the relationship between the force, F, and the time, t, observed in Fig. 7(a) for the slow-compression in each cycle is, $F(t) = -EALn(1 - vt/L_i)$, where A is the area of the sample perpendicular to the direction of compression. Thus, the rise of F during compression is dependent on many parameters: E, A, $L_i$, and $v$. However, from Fig. 8(a) it is clear that the composites display a remarkable elastic behavior because the same magnitude of force was required to achieve a 30% strain in consecutive cycles of compression. This behavior was observed in all of the prepared composites, regardless of the nanoparticle concentration or the direction of compression ($\parallel$ or $\perp$).

The L versus P curve, illustrated in Fig. 8(b), was obtained using the preceding relationships and the data from the F versus t curves. All of the L versus P curves were fitted by a single exponential with excellent correlations for pressures larger than 0.5 KgF/cm$^2$, that is, $L_{\parallel}(P) = \exp(-P/E_{\parallel})$ and $L_{\perp}(P) = \exp(-P/E_{\perp})$, showing that the composites follow Young's law in the range of applied strains for both orientations of the needles (the points associated with the lowest pressures, $P < 0.5$ KgF/cm$^2$, were neglected for fitting because they are influenced by instrumental factors related to the adjustment of the compression probe when contacting the sample). The values of $E_{\parallel}$ and $E_{\perp}$ were recovered from those fits for samples of composites with 10% *w/w* in $CoFe_2O_4$, obtaining $E_{\perp}$ at about 5 KgF/cm$^2$ and $E_{\parallel}$ between 15 and 20 KgF/cm$^2$, depending on the sample. It must be remarked upon that the absolute values of Young's modulus are influenced by details related to sample preparation, which are not easy to match perfectly: weighted amounts of base and cross-linker, time and temperature of curing, intensity of the magnetic field, mass of the magnetic nanoparticles, ambient humidity, etc. For these reasons, intersample comparison of the absolutes values of Young's modulus for different samples is not a direct indicator of magneto-elastic effects. The concept to be remarked upon is that care must be taken when comparing Young's modulus (E) between samples because the factors mentioned are not easy to control and have an influence on the elastic properties. Therefore, variations in the values of E can be due to many sample preparation factors, most of which have been mentioned in the preceding sentence. On the contrary, the ratio ($E_{\parallel}/E_{\perp}$) for a given sample is less influenced by those factors, being a better candidate than the absolute values of $E_{\parallel}$ and $E_{\perp}$ for discussing tendencies. Values of ($E_{\parallel}/E_{\perp}$) between 3 and 4 were obtained for different replicates of the 10% *w/w* composites prepared in the presence of the magnetic field, demonstrating the induction of elastic anisotropy.

Concerning the absolute values of Young's modulus, we always recovered values of $E_{\parallel}$ systematically larger than those obtained for Young's modulus of samples cured in the absence of an applied magnetic field, and the recovered values of $E_{\parallel}$ and $E_{\perp}$ are in the range of reported values for PDMS non-structured films; between 2.8 and 10 KgF/cm$^2$.[24,33] To our knowledge, this is the first time that values of the anisotropic Young's modulus are reported for magnetically induced structured composites. The values of $E_{\parallel}$ and $E_{\perp}$, calculated in different cycles, remain the same with good partial recovery and no elastic hysteresis, thus confirming that all the prepared composites behave as elastic materials, as was observed in Fig. 8(a).

The main aspect to be remarked upon is the induction of strong anisotropic effects, that is, ($E_{\parallel}/E_{\perp}$) > 1 (between 3 and 4 under the present conditions) for all of the prepared samples, in concordance with previous reports.[34] This ratio always rendered values between 3 and 4 for intra-sample comparison, indicating the induction of anisotropic elastic properties by the magnetic field during curing.

Figure 8(c) shows the responses for different composites that were compressed up to a maximum stress, and then the penetration distance was kept fixed for 60 s after reaching the fixed compression. It is observed that the pressure remains almost fixed at the initial value for all of the samples, with a slight decrease of about 10% after the 60 s of compression. As a corollary, the structure showed recovery after compression. This finding is, again, in agreement with the results shown in Fig. 8(a), that is, the material has a highly elastic behavior in spite of the presence of the inorganic needles.

## IV. CONCLUSIONS

In this work, the potential of ferro (magnetically blocked) and superparamagnetic nanoparticles of cobalt-iron oxides to produce magnetoelastomer structured composites in PDMS was explored. It was experimentally verified that the application of a uniform magnetic field of moderate intensity during curing induces the formation of needle-like-shaped macroscopic structures, with lengths on the order of hundreds of microns oriented in the direction of the field. This effect was only observed in the case of using ferromagnetic nanoparticles with a mean size larger than or equal to 10 nm, and are not observed when using the smallest nanoparticles (2 nm, which are in the superparamagnetic state at room temperature). Thus, the formation of needles is directly related to the size of the nanoparticles, which determines the magnetic properties.

Characterization studies carried out by SEM, VSM, and FMR indicate that needle-shaped structures are composed of aggregates of individual nanoparticles which preserve their original size, shape, and magnetic state. The structured composites made with nanoparticles in the ferromagnetic state retain the ferromagnetic nature of the filler particles without a change in the coercive field. At the same time, the composite structure has a moderate magnetic anisotropy (under the experimental conditions used in this work), such as a 25% increase of the remanence magnetization (normalized by the saturation magnetization) in the direction parallel to the structure axis with respect to the perpendicular one. The magnetic anisotropy was confirmed by (preliminary) experiments of FMR.

The elastic nature of the composite is not destroyed; not by the presence of the filler particles (at least up to 10% *w/w*) or by the induction of structuring. That is, both isotropic and structured composites have excellent elastic properties, including zero hysteresis, mechanical relaxation times on the order of tenths of seconds, and the possibility to perform many cycles of compression-decompression without changing Young's modulus. The structured composites have anisotropic values of the Young's modulus with values of the

ratio ($E_{\|}/E_{\perp}$) about 3 and 4 under the experimental conditions tested here ($E_{\|}$ and $E_{\perp}$ refer to the directions parallel and perpendicular to the needles, respectively).

In summary, from the results presented here, a physical image of the structured ferromagnetic $CoFe_2O_4$-PDMD composites clearly emerges. The first observation is that even though the particles are grouped into macroscopically anisotropic structures, they retain their individual properties intact, such as shape and size, ferromagnetic character, and low magnetic anisotropy of the domains. Nevertheless, when considering both magnetic and elastic properties of the material, it is established that the anisotropic grouping (needles) results in the appearance of both magnetic and elastic anisotropy of the material as a whole. This is produced without loss of the elastic nature of the composite, which (under the experimental conditions tested here) are provided by the elastomeric polymer. While the research of the various aspects and topics presented here should be deepened in future works, mainly by varying the intensity of the applied field, extending the range of concentrations of nanoparticles, and the chemical nature of polymer used and/or its degree of cross linking, the above description appears as a well-defined characterization for the composites of $CoFe_2O_4$ nanoparticles in PDMS. To the best of our knowledge, this is the first time that these effects are reported for the case of nanoparticles of cobalt-iron oxides, considering particles with super-para- and ferromagnetic behavior, in a cured non-fluid polymer. These results must be taken into account when considering its application in magnetoelastomer-based devices.

## ACKNOWLEDGMENTS

P.S.A. is a postdoctoral fellowship of the National Council of Research and Technology (CONICET, Argentina). G.J., A.B., and R.M.N. are research members of CONICET. Financial support was received from the University of Buenos Aires (UBACyT 2008-2010, Project X157), Agencia Nacional de Promoción Científica y Tecnológica (Grant Nos. PICT 2006-00568 and PICT 2006-01201) and CONICET (Grant No. PIP 6382). The authors thank the Center of Documental Production (CePro, School of Sciences, University of Buenos Aires) for obtaining the presented pictures.

[1]S. Glenis, V. Likodimos, N. Guskos, D. Yarmis, G. Zolnierkiewicz, A. Szymczyk, and C. L. Lin, J. Appl. Phys.**108**, 054314 (2010).
[2]G. Diguet, E. Beaugnon, and J. Y. Cavaille. J. Magn. Magn. Mater. **321**, 396 (2009).
[3]O. T. Mefford, M. R. J. Carroll, M. L. Vadala, J. D. Goff, R. Mejia-Ariza, M. Saunders, R. C. Woodward, T. G. St. Pierre, R. M. Davis, and J. S. Riffle, Chem. Mater. **20**, 2184 (2008).
[4]G. V. Stepanov, S. S. Abramchuk, D. A. Grishin, L. V. Nikitin, E. Yu. Kramarenko, and A. R. Khokhlov, Polymer **48**, 488 (2007).
[5]G. Filipcsei, I. Csetneki, A. Szilágyi, and M. Zrinyí, Adv. Polym. Sci. **206**, 137 (2007).
[6]Z. Varga, G. Filipcsei, and M. Zrınyí, Polymer **47**, 227 (2006).
[7]Z. Varga, G. Filipcsei, and M. Zrınyí, Polymer **46**, 7779 (2005).
[8]A. Lappas, A. Zorko, E. Wortham, R. N. Das, E. P. Giannelis, P. Cevc, and D. Arc, Chem. Mater. **17**, 1199 (2005).
[9]D. L. Huber, J. E. Martin, R. A. Anderson, D. H. Read, and B. L. Frankamp, Sandia Report No. SAND2005-8032, U.S. Department of Energy, 2005, pp.1–103.
[10]K. Keshoju and L. Sun, J. Appl. Phys. **105**, 023515 (2009).
[11]M. R. Jolly, J. D. Carlson, and B. C. Muñoz, Smart Mater. Struct. **5**, 607 (1996).
[12]M. Farshad and A. Benine, Polym. Test. **23**, 347 (2004).
[13]H. Denver, T. Heiman, E. Martin, A. Gupta, and D.-A. Borca-Tasciuc, J. Appl. Phys. **106**, 64909 (2009).
[14]S. E. Jacobo, J. C. Aphesteguy, R. Lopez Antón, N. N. Schegoleva, and G. V. Kurlyandskaya, Eur. Polym. J. **43**, 1333 (2007).
[15]N. Kchit and G. Bossis, J. Phys.: Condens. Matter **20**, 204136 (2008).
[16]L. Lanotte, G. Ausanio, C. Hison, V. Iannotti, and C. Luponio, Sens.Acuators, A **106**, 56 (2003).
[17]C. N. Chinnasamy, M. Senoue, B. Jeyadevam, O. Perales-Perez, K. Shinoda, and K. Tohji, J. Colloid Interface Sci. **263**, 80 (2003).
[18]T. Meron, Y. Rosenberg, Y. Lereah, and G. Markovich, J. Magn. Magn. Mater. **292**, 11 (2005).
[19]M. P. Gonzalez-Sandoval, A. M. Beesley, M. Miki-Yoshida, L. Fuentes-Cobas, and J. A. Matutes-Aquino, J. Alloys Compds. **369**, 190 (2004).
[20]Y. I. Kim, D. Kim, and C. S. Lee, Physica B **337**, 42 (2003).
[21]S. D. Sartale and C. D. Lokhande, Ceram. Int. **28**, 467 (2002).
[22]V. Pillai and D. O. Shah, J. Magn. Magn. Mater. **163**, 243 (1996).
[23]Y. Qu, H. Yang, N. Yang, Y. Fan, H. Zhu, and G. Zou, Mater. Lett. **60**, 3548 (2006).
[24]R. M. Negri, S. D. Rodriguez, D. L. Bernik, F. V. Molina, A. Pilosof, and O. Pérez, J. Appl. Phys. **107**, 113703 (2010).
[25]S. C. Goh, C. H. Chia, S. Zakaria, M. Yusoff, C. Y. Haw, Sh. Ahmadi, N. M. Huang, and H. N. Lim, Mater. Chem. Phys. **120**, 31 (2010).
[26]C. H. Chia, S. Zakaria, M. Yusoff, S. C. Goh, C. Y. Haw, Sh. Ahmadi, N. M. Huang, and H. N. Lim, Ceram. Int. **36**, 605 (2010).
[27]W. S. Chiu, S. Radiman, R. Abd-Shukor, M. H. Abdullah, and P. S. Khiew, J. Alloys Compds. **459**, 291 (2008).
[28]D. L. Leslie-Pelecky and R. D. Rieke, Chem. Mater. **8**, 1770 (1996).
[29]M. Vásquez Mansilla, J. Gómez, E. Sallica Leva, F. Castillo Gamarra, A. Asenjo Barahona, and A. Butera, J. Magn. Magn. Mater. **321**, 2941 (2009).
[30]V. Blaskov, V. Petkov, V. Rusanov, L. M. Martinez, B. Martinez, J. S. Muñoz, and M. Mikhov J. Magn. Magn. Mater. **162**, 331 (1996).
[31]A. Butera, Eur. Phys. J. B **52**, 297 (2006).
[32]A. Boczkowska, S. F. Awietjan, T. Wejrzanowski, and K. J. Kurzydlowski, J. Mater. Sci. **44**, 3135 (2009).
[33]F. Carmona, R. Canet, and P. Delhaes, J. Appl. Phys. **61**, 2550 (1987).
[34]T. Hajsz, I. Csetneki, G. Filipcsei, and M. Zrinyí, Phys. Chem. Chem. Phys. **8**, 977 (2006).
[35]See supplementary material at http://dx.doi.org/10.1063/1.3624602 for device design, histograms, and SEM images.